# Transfer function analysis of measured transfer matrices

Shao Yang, I. P. Vayshenker, Dag R. Hjelme, and Alan R. Mickelson

Measurements of mode transfer matrices of various multimode fiber optic connectors are presented. To analyze the accuracy and repeatability of such measurements, a theoretical framework which employs mode transmission functions is derived. It is shown that the transfer function can be used to find transfer matrices for any set of launches. A procedure for determination of the mode transfer function is given.

## I. Introduction

Multimode fiber systems are not describable in terms of the results of simple loss measurements alone. Mode dependent transmission by fiber system components such as splices, connectors and splitters, as well as mode dependent attenuation, causes the modal power distribution to vary with propagation distance along the system propagation path. As component intensive systems such as local area nets (LANs) and premises wiring do not include the great fiber lengths that are necessary to achieve steady state power distribution (probably several kilometers), the modal power distribution in such a system will remain in a transient state. There is therefore no standard launch that can be used to determine typical loss values. Although it is clear that overfilled loss measurements would lead to much too pessimistic loss values, differences between the associated steady state modal distribution for other components do not allow one to select a lower bound loss excitation.

The above considerations indicate that one needs to analyze multimode systems with a tool which carries some information concerning the evolution of the modal power distribution through the system. Holmes proposed just such a tool in 1981 in a paper in which he introduced the mode transfer matrix.[1] The idea of the mode transfer matrix was that the input and output power distributions could be arbitrarily quantized into power vectors that could then be related by a transfer matrix. Indeed, this tool was later successfully applied to the prediction of loss in fusion splices,[2] microbends,[3] connectors,[4] and power splitters[5] as well as to the prediction of system bandwidth.[6]

A potential problem with the mode transfer matrix approach arises from the fact that Holmes's[1] original definition of the matrix as being that matrix which relates the input power vector to the output power vector is not an operational definition in the sense that the matrix cannot be experimentally determined from its definition. Specification of the $N$ components of the input power vector and measurement of the $N$ components of the output power vector cannot provide sufficient information for the determination of the $N^2$ elements of the transfer matrix. In practice, a determination of the matrix must require the selection of $N$ independent launches and the measurement of the $N$ components of the output vector for $N$ different (known) input vectors. This is the procedure that has been used in the literature.[2-6] Unfortunately, though, the definition of the transfer matrix yields no information regarding how to choose the $N$ input launches nor, for that matter, any information concerning what would constitute $N$ independent launches. However, these questions are crucially important in determining the ultimate accuracy and repeatability of the transfer matrix approach.

The electromagnetic theory of guided wave propagation does yield some information on how transfer matrices should be chosen. For example, in the coupled mode theory of Marcuse,[7] the transition matrix is a complex-valued matrix which relates the amplitude and phase of each mode excitation coefficient at the input and output of a fiber section. As Marcuse himself states, however, this amount of information is generally unnecessary and he proceeds to derive coupled power equations.[7] Indeed, if one excites a multimode fiber with a coherent source, one rapidly finds out that one would rather not have phase information carried by the modes, as the result is speckled near

When this work was done all authors were with University of Colorado, Department of Electrical & Computer Engineering, Boulder, Colorado 80309-0425; I. P. Vayshenker is now with U.S. National Institute of Standards & Technology, Optical Metrology Group, Boulder, Colorado 80303.

Received 29 August 1988.
0003-6935/89/153148-10$02.00/0.

fields and modal noise.[8] As was shown in Ref. 9, use of multimode or incoherent excitation of a multimode fiber leads to the excitation of a continuum of modes and therefore an averaging out of phase information. As a continuum of modes is excited, one can pass mode sums to integrals and represent modal excitation coefficients in terms of a function of a single continuous parameter. This function is generally referred to as a modal power distribution which is a function of the mode parameter. In this picture, an output distribution can be represented as an integral operator operating on an incident distribution. The kernel of this operator is the transfer function. This transfer function can therefore be taken as the object which represents given fiber components, at least in practical systems where the mode continuum approximation applies.

In the mode continuum approximation where a transfer function can be used to completely characterize a component, transfer matrices appear as truncated projections of the transfer function. To perform a projection, one must choose a basis. Such is the problem of choosing a set of independent launches. As will be shown in the following development, though, a serious problem arises in that the transfer matrix turns out to be a weighted average of the transfer function, with the weight being the incident power distribution. This is a serious failing of the transfer matrix, as several incident distributions are necessary for its determination. This leads to a situation in which the values of the on-diagonal matrix elements have a higher accuracy than those off-diagonal. It further leads to a situation in which there is no unique transfer matrix unless the launch conditions are specified in detail. Errors incurred in generating these specified launches are serious, as they affect not only the accuracy to which the desired result is perturbed but perturb the desired result itself.

In the present work, we try to assess the uncertainty of the transfer matrix method by using the transfer function as a tool. Relations between the transfer matrix and transfer function will be derived. A general form for the transfer function is presented and a form for the undetermined coupling function contained in the transfer function is proposed. Experimentally determined transfer matrices will be analyzed using this transfer function approach. The development will naturally lead to concepts suggesting an improved measurement approach. The paper is organized as follows: Section II contains a short review of the mode continuum approximation, thereby defining the quantities and symbols to be used in the later presentation. Section III contains a presentation of the experimental results. Section IV presents the main theoretical results of this work. Section V contains a transfer function analysis of the experimental results. The last section contains conclusions.

## II. Transfer Function Theory

To aid in interpretation of the experimental results as well as to serve as a basis for later theory, this section of the paper contains the basic relations used in transfer function theory. A basic tenet behind the use of transfer function theory is that the modes of the fiber actually form a continuum. This is a condition on the linewidth, $\delta\lambda$, of the source of center wavelength $\lambda$. As was derived in Ref. 9, the inequality to be satisfied for the mode continuum approximation to hold is

$$\frac{\delta\lambda}{\lambda} \geq \frac{\sqrt{2\Delta}}{N_1 ka}, \tag{1}$$

where $\sqrt{2\Delta}$ is the index contrast which can be defined by the fiber profile

$$n(r) = \begin{cases} n_1\left[1 - 2\Delta f\left(\frac{r}{a}\right)\right]^{1/2} & r < a, \\ n_1[1 - 2\Delta]^{1/2} & r > a, \end{cases} \tag{2}$$

where $f(r/a)$ is the profile function, $a$ is the fiber core radius, $k = 2\pi/\lambda$ is the mean propagation constant, $n_1$ is the axial refractive index, and $N_1 = n_1 - \lambda dn_1/d\lambda$ is the axial group index. Were Eq. (1) not to hold, actually two problems would arise. Clearly, for small enough linewidths, modal noise would arise and it would become necessary to keep track of all the phases of all the modes, something that transfer function theory does not do. Second, if Eq. (1) is violated, the theory could not be expressed in terms of continuum concepts. More will be said about this as we proceed.

If Eq. (1) is satisfied, a modal power distribution $p(R)$ can be defined by

$$p(R) = -\frac{2\pi}{V^2}\frac{1}{\partial f/\partial s}\frac{\partial I}{\partial s}\bigg|_{s=f^{-1}(R)}, \tag{3}$$

where the dimensionless radial coordinate $s = r/a$, the fiber $V$ number is given by $V^2 = 2\Delta k_1 a$ where $k_1 = n_1 k$, $I(s)$ is the near field intensity of the fiber, $f^{-1}$ is the inverse function to the profile function $f$, and $R$ is the mode parameter. The mode parameter can either be expressed in terms of the modal propagation constant $\beta$ by

$$R^2 = \frac{1}{2\Delta}\left[1 - \frac{\beta^2}{n_1^2 k^2}\right], \tag{4}$$

or, by using geometrical optics, in terms of the ray tracing parameters $s = r/a$ and $\theta$ (the angle a ray makes with the $z$ axis) by

$$R^2 = s^2 + \frac{\sin^2\theta}{2\Delta}. \tag{5}$$

It is easily shown that $R$ is a constant of the motion along a ray path in sufficiently weakly guiding fibers.

$p(R)$ is an important function in that practically any quantity of interest about the fiber can be calculated in terms of it. For example, the near field intensity is expressible as

$$I(s) = \frac{V^2}{\pi}\int_{f^{1/2}(s)}^{1} p(R)RdR, \tag{6}$$

and the total power carried by the fiber as

$$P = \int_0^1 p(R)m(R)dR, \tag{7}$$

where $m(R)$ is the modal density and is given by

$$m(R) = V^2 R\left[\frac{f^{-1}(R^2)}{a}\right]^2. \tag{8}$$

The essence of transfer matrix theory goes back to a work of Holmes,[1] and the basic tenet is that a component can be represented by a matrix. To do this, one has to represent the power incident on the component by a vector $\mathbf{P}^i$ and the power exiting by a vector $\mathbf{P}^o$. The transfer matrix can then be defined by the matrix relation

$$\mathbf{P}^o = \boldsymbol{T}\mathbf{P}^i, \tag{9}$$

where, using Eq. (7), we can make the identifications

$$\mathbf{P}^o = \begin{bmatrix} P_{01} \\ P_{02} \\ . \\ . \\ P_{on} \end{bmatrix}, \quad \mathbf{P}^i = \begin{bmatrix} P_{i1} \\ P_{i2} \\ . \\ . \\ P_{in} \end{bmatrix}, \tag{10}$$

and

$$P_j^o = \int_{R_{j-1}}^{R_j} p^o(R)m(R)dR \quad \text{for } 1 \le j \le n, \tag{11a}$$

$$P_j^i = \int_{R_{j-1}}^{R_j} p^i(R)m(R)dR \quad \text{for } 1 \le j \le n, \tag{11b}$$

where $R_o = 0$ and $R_n = 1$, and the others can be chosen as one wishes. Evidently, although Eq. (9) defines $\boldsymbol{T}$, it is not sufficient to solve for $\boldsymbol{T}$. We need $N$ more relations of $N$ equations to define the $N^2$ components of $\boldsymbol{T}$. By making $N$ independent excitations, however, we can form matrices $\boldsymbol{P}^o$ and $\boldsymbol{P}^i$ according to the rule

$$\boldsymbol{P}^o = [\mathbf{P}_1^o, \mathbf{P}_2^o, \ldots \mathbf{P}_n^o] \quad \boldsymbol{P}^i = [\mathbf{P}_1^i, \mathbf{P}_2^i, \ldots, \mathbf{P}_n^i], \tag{12}$$

where the $\mathbf{P}_j^o(\mathbf{P}_j^i)$ is the output (input) vector for the $j$th independent excitation. With these matrices, one can now write the analog of Eq. (9):

$$\boldsymbol{P}^o = \boldsymbol{T}\boldsymbol{P}^i, \tag{13}$$

which can be solved for $\boldsymbol{T}$ to yield

$$\boldsymbol{T} = \boldsymbol{P}^o[\boldsymbol{P}^i]^{-1}. \tag{14}$$

A final point should be made before going on to the discussion of the experiment. Clearly, the choice of the discretization of Eq. (11) appears to be somewhat arbitrary, as there seems to be no rule on how to discretize. But in fact, if Eq. (1) is satisfied, we really do have a mode continuum and we need not discretize. We could just as well define a transfer function $T(R,R')$:

$$p^o(R)m(R) = \int_0^1 T(R,R')p^i(R')m(R')dR' \tag{15}$$

and the associated transfer operator is defined by

$$P^o(R) = \hat{T}P^i(R), \tag{16}$$

where

$$P^o(R) = p^o(R)m(R), \tag{17a}$$

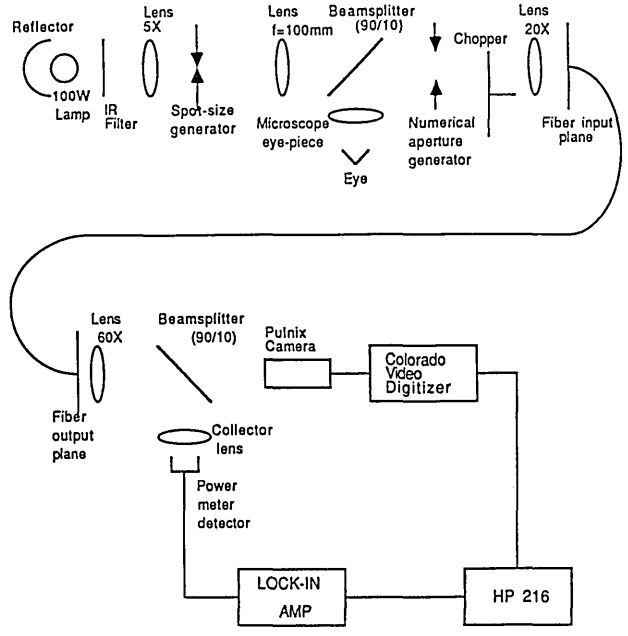


Fig. 1. Schematic depiction of the experimental apparatus used to measure the mode transfer matrices used in this paper.

$$P^i(R) = p^i(R)m(R). \tag{17b}$$

It is just such a viewpoint that we take later on in the development.

## III. Experiment

The experimental apparatus is depicted in Fig. 1. A 100-W halogen lamp with an ellipsoidal reflector was used as the source. The light source is focused onto a spot size generator by means of 5× microscope lens. The combination of the lens of 100-mm focal length and input microscope lens of 20× magnification produces a demagnification of 10.96, since the focal length of the 20× lens is 9.12 mm. To select the range of the wavelengths, an infrared bandpass filter with center wavelength of 850 nm and a passband of 50 nm was employed. The spot size generator consists of three patterns. The first is a small hole with a diameter of 100 $\mu$m which is used for central excitation; the second is used for off-central excitation and is an annulus which has an outer diameter of ~688 $\mu$m and an opaque center circle with a diameter of 525 $\mu$m; and the third is a large hole with a diameter of ~1.5 mm which is used for overfilled excitation. The fiber end is easily viewed by means of the microscope, which also allows measurement of the spot size of the launched beam as well as of the core diameter.

In the receiving system, the fiber output is imaged with a 60× microscope lens into a Pulnix TV camera. The beam splitter allows 90% of the output to be transmitted to the camera channel and 10% to the power meter detector. This configuration allows most of the energy to be transmitted to the camera channel, since the power meter channel does not require a large amount of signal with the high lock-in amplifier sensitivity. The Pulnix camera is a charge-coupled device

(CCD) array camera which produces resolution in the horizontal direction of 280 TV lines and in the vertical direction of 350 TV lines. The near field intensity is then digitized with the use of a solid state video memory (Colorado Video 491 Frame Store) with high speed A–D and D–A converters and is capable of digitizing, storing, and displaying a single frame of video information. This unit utilizes standard 2:1 interlace and dot interlace to increase horizontal resolution. A model 793 I/O module is installed in the 491 Video Frame Store, which provides interfacing to a Hewlett-Packard HP 216 personal computer.

Power measurements are critical in obtaining the transmission matrices. To obtain the most accurate power measurements, the software is written in such a way that 100 power measurements are averaged. Also, the near field intensity measurement requires some caution. Here, the software is written such that the total near field intensity can be averaged from up to eighty measurements. This technique is much superior to the one used in mechanical scanning setups, since the high accuracy is achieved by simple and fast averaging. The speed of the system minimizes noise producing effects of thermal variation.

In line with the design of the spot generator, we chose to measure 2 × 2 matrices. The general experimental procedure was as follows. First, a 1-m length of fiber was placed at the input location. The input end of this fiber was not moved following its initial placement. The output of this fiber with the central excitation as the input then served as a reference. The component under test, with a 1-m fiber pigtail at its output, was then attached to the reference fiber output without a change in the excitation. That the excitation was not changed is rather important since it is very complicated to return to a given excitation during a measurement series. By not trying to return to a given launch, one can greatly improve one's measurement error on a given component. After measuring the output for central excitation, the component output is measured for overfilled excitation and then for noncentral excitation. The component is then removed, and the reference output for the noncentral excitation is recorded. The overfilled excitation is then repeated. It is deemed that this excitation is repeatable. The reference output is then recorded for this overfilled excitation.

The data were then processed by a fitting procedure. One could use Eq. (3) to convert the near fields to modal power distributions. However, numerical differentiation of experimental data is a very error-prone operation. Instead, the following forms

$$p(R) = A \exp(-\Omega R), \tag{18a}$$

$$p(R) = AR^2 \exp(-\Omega R^4) \tag{18b}$$

were chosen, Eq. (18a) for central excitation and Eq. (18b) for noncentral, where $A$ and $\Omega$ are free parameters. The $A$ and $\Omega$ parameters could be determined by overfilled loss measurement and by the use of Eq. (7) to fit the measured near field. An $R_1$ value for use in Eq. (11) was then selected, and Eq. (14) was used to determine the 2 × 2 **T** matrix.

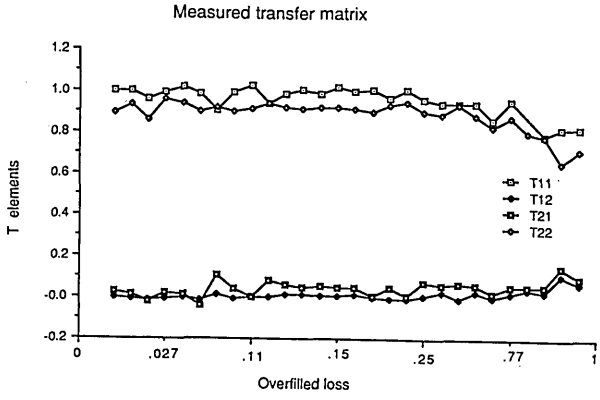


Fig. 2. Plot of the elements of the transfer matrix, measured by a two excitation technique, for a connector in various states of connection as a function of their overfilled loss.

Figure 2 illustrates the main measurement results. Plotted here are the elements of the **T** matrix as a function of the overfilled loss for a connector in various states of connection. Table I summarizes launch data for the sets of connection states used for the various launches. In the table the $D$ denotes the average (over the ensemble) deviation from the mean, as defined by the curve used to fit the data. The $S$ is the standard deviation from this curve. The launches are characterized by their $k$ values, where the $k$ are defined by

**Table I. Statistics of Six Groups of Experimental Data, each Group having the Same Launch Condition denoted by $k_1$ and $k_2$ where $D$ is the Mean Deviation of the Data in each Group from the Fitted Curve and $s$ is the Standard Deviation, with the Last Column Showing the Statistical Results for all the Data in the Six Groups**

| | | 1 | 2 | 3 | 4 | 5 | 6 | Total |
|---|---|---|---|---|---|---|---|---|
| K1($P_{11}^i/P_{21}^i$) | | 2.41 | 4.46 | 2.96 | 2.92 | 0.06 | 2.1 | |
| K2($P_{22}^i/P_{12}^i$) | | 4.55 | 4.21 | 6.40 | 2.26 | 2.27 | 1.05 | |
| T11 | D | .0139 | .0059 | .0008 | -.0293 | .0084 | .0127 | 0 |
| | S | .0302 | .0059 | .0537 | .037 | .027 | .0156 | .0358 |
| T12 | D | -.0068 | -.0043 | -.0064 | .0021 | .0069 | .0168 | 0 |
| | S | .0076 | .0052 | .0118 | .02 | .0078 | .0357 | .0153 |
| T21 | D | -.0082 | -.0144 | -.018 | .0045 | .0201 | .0192 | 0 |
| | S | .0252 | .0162 | .0495 | .0246 | .023 | .043 | .0325 |
| T22 | D | .0064 | -.0039 | .0097 | -.012 | .0053 | -.0241 | 0 |
| | S | .0202 | .0214 | .0379 | .0234 | .0106 | .0591 | .0286 |

Fitted curve

T11 $y=.992-.2055x^{1.6}$

T12 $y=.0022+.0912x^{4.9}$

T21 $y=.0369+.095x^{6.7}$

T22 $y=.9159-.2603x^{3.8}$

$$k_1 = \frac{P^i_{11}}{P^i_{21}}, \tag{19a}$$

$$k_2 = \frac{P^i_{22}}{P^i_{12}}, \tag{19b}$$

where the $P^i_{jk}$ are the elements of the matrix defined in Eq. (12).

As stated above, the measurements were all carried out for a single connector in various states of connection. The idea behind this was that each time the connector was pulled apart and reconnected, the difference between this reconnection and the original connection would be as different as the differences between two different connectors in similar states of connection. This assumption has not been studied in any detail, but hopefully is true for well assembled connectors.

An interesting point that can be surmised from the study of either Fig. 2 or Table I is that the standard deviations of the elements are more or less independent of their mean values. That is to say that the relative uncertainties in the $T_{12}$ and $T_{21}$ elements are much greater than in the diagonal elements. This is not too surprising if one studies Eq. (14) for the **T** matrix. All the values of the powers, both big and small, go into the calculation of the **T** matrix elements. Therefore the relative error will be relative to the largest power value. One could assume that this is the cause of some of the seemingly unphysical negative values of the $T_{12}$ elements pictured in Fig. 2. However, as will be seen later in this paper, negative values of matrix elements need not arise only due to noise, but can also be caused by the choice of launches themselves, and negative values could even arise in the absence of noise. This point will be discussed later in this work.

## IV. Theory

What we wish to do here is to establish relationships between the transfer function and the transfer matrix for purposes of elucidating the actual meaning of the measured results. Here, the point of view that the transfer function is the mathematical object which represents the test component will be taken. This seems to be a rational point of view to take if it is to be tacitly assumed that the mode continuum approximation applies. Therefore, the equation which defines the effect of a component is Eq. (15). To find a matrix corresponding to the operator $T$ of Eq. (16), one needs to choose an orthogonal basis of functions $\varphi_k(R)$. If one does this, one finds that

$$T_{jk} = \frac{1}{E_k}\int_0^1 dR\varphi_j(R)\hat{T}\varphi_k(R), \tag{20}$$

where

$$E_k = \int_0^1 dR\varphi_k^2(R), \tag{21}$$

with the power vectors of Eq. (11) now given by

$$P^o_j = \int_0^1 dRp^o(R)m(R)\varphi_j(R), \tag{22a}$$

$$P^i_j = \int_0^1 dRp^i(R)m(R)\varphi_j(R). \tag{22b}$$

Whereas in Eqs. (9)–(11) it was assumed that the power vectors could be chosen of an arbitrary length $n$, here it is evident that the power vectors are infinite dimensional as it takes an infinite number of functions $p(R)$ to span the space $0 \le R \le 1$. To hook up with the $2 \times 2$ representation, however, one could choose

$$\varphi_{2j+1} = \frac{1}{m(R)}\begin{cases} a_{2j+1}\cos\left(R - \dfrac{R_c}{2}\right)\dfrac{2\pi}{R_c} \\ a_{2j+1}\sin\left(R - \dfrac{R_c}{2}\right)\dfrac{2\pi}{R_c} \end{cases}$$

$$0 < R < R_c \quad j = 0,1,2\ldots, \tag{23a}$$

$$\varphi_{2j} = \frac{1}{m(R)}\begin{cases} b_{2j}\cos\left(R - \dfrac{1+R_c}{2}\right)\dfrac{2\pi}{1-R_c} \\ b_{2j}\sin\left(R - \dfrac{1+R_c}{2}\right)\dfrac{2\pi}{1-R_c} \end{cases}$$

$$R_c < R < 1 \quad j = 1,2\ldots, \tag{23b}$$

which is just a double Fourier series, one on $[0,R_c]$ and one on $[R_c,1]$. The first terms of $\varphi_1(R)$ and $\varphi_2(R)$ would just be rectangle functions which have value unity on the two intervals, respectively. Therefore, the values of $T_{jk}$ for $j,k = 1,2$, and the first two elements of the power vectors would be exactly those which would be defined for a $2 \times 2$ case from Eqs. (9)–(11). Unfortunately, there are still a countable infinity of terms left over. To clarify what these other terms do, one picks a set of $n$ excitations. One can then choose input and output matrices as per Eq. (12). These matrices will now have dimension $\infty \times n$. Clearly, Eq. (14) will still hold except that now the transfer matrix will have dimensions of $\infty \times \infty$. If one had the correct power matrices, one could perform the operations of Eq. (14) and then truncate to $n \times n$ to obtain a transfer matrix we will denote by $\boldsymbol{T}^e$, meaning the exact $\boldsymbol{T}$. However, in practice one does not determine the exact power matrices but uses truncated $n \times n$ versions $\boldsymbol{P}^{oT}$ and $\boldsymbol{P}^{iT}$ to determine the measured transfer matrix $\boldsymbol{T}^m$. This operation is not the same as calculating directly, as can be noted by writing

$$\boldsymbol{T}^{(m)} = \boldsymbol{P}^{oT}(\boldsymbol{P}^{iT})^{-1} = \boldsymbol{T}^e + \boldsymbol{T}^+\boldsymbol{P}^{i+}(\boldsymbol{P}^{it})^{-1}, \tag{24}$$

where $\boldsymbol{T}^+$ is the transfer matrix with the first $n$ columns replaced by zero vectors and $\boldsymbol{P}^{i+}$ is the excitation matrix with its first $n$ rows replaced by zeros, a situation illustrated in Fig. 3.

A major point of the above argument is that the truncation of the power matrices causes an added error. The only way this error can be made to go away is if the $\boldsymbol{P}^{i+}$ is identically zero. Recalling Eq. (22), this could only be the case if

$$\int_o^1 dRp^i(R)m(R)\varphi_j(R) = 0, \quad \forall\, j > n, \text{ and } p^i(R), \tag{25}$$

that is, if all the $n$ excitations were orthogonal to all the basis functions. Recalling the double Fourier series example of Eq. (23) as applied to a 2 × 2 case, the two excitations would have to be perfectly flat modal distributions, the first flat between 0 and $R_c$ and the second flat from $R_c$ to 1. This is what is meant by independent excitations. They cannot overlap and must be orthogonal to all higher order terms. Unfortunately, the diffraction limit precludes us from actually generating such launches.

Now that it has been determined what is meant by the term independent launches, it is time to try to assess how serious it is that such launches cannot quite be generated. For simplicity, we consider only a 2 × 2 case. Clearly, the power exiting a component can be expressed in the form

$$P^o = P_1^o + P_2^o = T_{11}P_1^i + T_{12}P_2^i + T_{21}P_1^i + T_{22}P_2^i. \tag{26}$$

A second expression for the power can be found by writing Eq. (7) in the form

$$\begin{aligned} P^o = &\int_0^{R_c} dR \int_0^{R_c} dR' T(R,R')m(R')p^i(R') \\ &+ \int_0^{R_c} dR \int_{R_c}^{1} dR' T(R,R')m(R')p^i(R'), \\ &+ \int_{R_c}^{1} dR \int_o^{R_c} dR' T(R,R')m(R')p^i(R') \\ &+ \int_{R_c}^{1} dR \int_{R_c}^{1} dR' T(R,R')m(R')p^i(R'). \end{aligned} \tag{27}$$

Now, as it has been previously stated, it is not clear how to perform the discretization of $T(R,R')$. A possible way is to identify each of the four terms of Eq. (27) with each of the four terms of Eq. (26). Although such a decomposition is not unique, it seems plausible and indeed, in the limit where one can generate arbitrary (possibly unphysical) launches, one can show that such a decomposition could actually be justified. Performing the decomposition, and using Eqs. (11) to express the incident power vectors, one obtains the following relations:

$$T_{11} = \frac{\int_0^{R_c} dR \int_0^{R_c} dR' T(R,R')m(R')p^i(R')}{\int_0^{R_c} dR' m(R')p^i(R')}, \tag{28a}$$

$$T_{12} = \frac{\int_0^{R_c} dR \int_{R_c}^{1} dR' T(R,R')m(R')p^i(R')}{\int_{R_c}^{1} dR' m(R')p^i(R')}, \tag{28b}$$

$$T_{21} = \frac{\int_{R_c}^{1} dR \int_0^{R_c} dR' T(R,R')m(R')p^i(R')}{\int_0^{R_c} dR' m(R')p^i(R')}, \tag{28c}$$

$$T_{22} = \frac{\int_{R_c}^{1} dR \int_{R_c}^{1} dR' T(R,R')m(R')p^i(R')}{\int_{R_c}^{1} dR' m(R')p^i(R')}, \tag{28d}$$

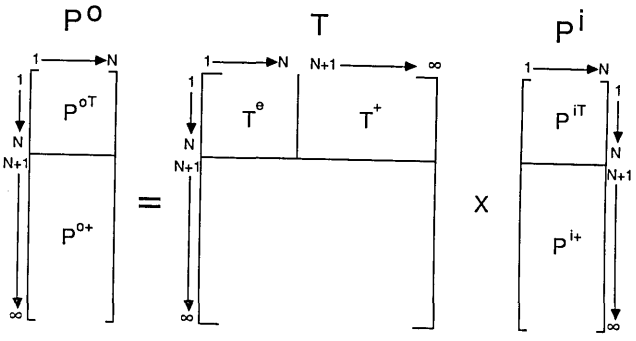


$$P^{oT} = T^e P^{iT} + T^+ P^{i+}$$

$$T_{(m)} = P^{oT}(P^{iT})^{-1}$$

$$= T^e + T^+ P^{i+}(P^{iT})^{-1}$$

Fig. 3. Schematic depiction defining the various matrices used in Eq. (24).

From Eq. (28) it is clear that the measured transfer matrix is simply a weighted average of the transfer function, where the weighting is given by the incident modal distribution. In practice, however, several launches are needed; it is not clear what information (28) gives us. Only in the flat launch limit, where the two launches are completely flat and nonoverlapping, will the above equations separate and $T_{11}$ and $T_{21}$ can be determined from one launch and $T_{12}$ and $T_{22}$ determined from the other. In the case that the two launches are not independent, it can be shown that

$$T_{11}^m = \frac{T_{11}^{(1)}k_1k_2 - T_{11}^{(2)} + [T_{12}^{(1)} - T_{12}^{(2)}]k_2}{k_1k_2 - 1}, \tag{29a}$$

$$T_{12}^m = \frac{T_{12}^{(2)}k_1k_2 - T_{12}^{(1)} + [T_{11}^{(2)} - T_{11}^{(1)}]k_1}{k_1k_2 - 1}, \tag{29b}$$

$$T_{21}^m = \frac{T_{21}^{(1)}k_1k_2 - T_{21}^{(2)} + [T_{22}^{(1)} - T_{22}^{(2)}]k_2}{k_1k_2 - 1}, \tag{29c}$$

$$T_{22}^m = \frac{T_{22}^{(2)}k_1k_2 - T_{22}^{(1)} + [T_{21}^{(2)} - T_{21}^{(1)}]k_1}{k_1k_2 - 1}, \tag{29d}$$

where the superscript $m$ refers to measured, the superscript 1(2) refers to the transfer matrix value determined from launch 1(2), and $k_1$ and $k_2$ are as they were defined in conjunction with Table I, in Eq. (19). As we've seen various times before, if the launches become flat and independent, i.e., if $k_1$ and $k_2 \to \infty$, the measured matrix becomes the truncated version of the exact. Otherwise, there will be a tendency for $T_{12}^{(m)}$ and $T_{21}^{(m)}$ to have very distorted values due to the fact that $T_{11}^{(m)}$ and $T_{22}^{(m)}$ tend to be much larger than the off-diagonal terms, yet they show up as error terms in Eqs. 28(b) and (c).

## V. Comparison with Experiment

It would be of great value to verify the result of Eq. (28). To do this, however, it is required that one know the transfer function. In this section of this paper, a form of the transfer function is presented and a two-parameter coupling function is proposed to close the model. As will be seen, the two coupling parameters can be determined from experimental data. This allows one to use the transfer function to derive various forms of the transfer matrix, such as the ones used in Eq. (20).

In a component such as the connector or splice, it seems quite safe to assume that the dominant loss mechanism will be mode coupling as the components are not long enough for there to be significant absorption or Rayleigh scattering. In this mode coupling case, there are only three things that can happen to the power in a mode. It can remain in that mode, it can be diminished by coupling out of that mode, or it can be augmented by coupling from other modes. With these considerations, one can see that the most general form a mode coupling driven transfer function can take is

$$T(R,R') = [1 - \int dR'' m(R'')\alpha(R'',R')]\delta(R - R') + m(R)\alpha(R,R'), \quad (30)$$

where $\alpha(R,R')$ is the coupling function. As coupling can be caused by a multitude of effects, it seems reasonable to assume that the coupling function could take the form of a Gaussian of the form

$$\alpha(R,R') = \tfrac{1}{2}\alpha_0 \exp(-|R^2 - R'^2|/2\tau), \quad (31)$$

where $\alpha_0$ and $\tau$ are fitting parameters. It is clear that the form of Eq. (31) cannot be good for all components or for that matter applicable for all values of $R$ and $R'$. For example, power coupled from an $R'$ to a value of $R > 1$ cannot be coupled back down as it is lost to the system. That power at $R > 1$ is lost to the system is taken into account by the limits on the integrals in Eqs. (7) and (15), the form of the coupling function that would allow down-coupling from $R > 1$ values. For small loss, this is probably acceptable, but there are limitations. These limitations are not in the form of Eq. (29) but of Eq. (30), and therefore there is always hope that a fix-up of Eq. (30) could improve the accuracy of the approach or allow the approach to be applied to a variety of different components. This will be left for future work.

Figures 4–6 illustrate some of the predictions of the transfer function of Eqs. (30) and (31). Figure 4 shows predictions of Eq. (29) for fixed $k_1$ and $k_2$ as a function of loss for fixed values of $\tau$. These plots should correspond to the data displayed in Fig. 2. Direct comparison is difficult, as the data of Fig. 2 was taken for various launch conditions. The trend of the data and that of the predictions of Fig. 4 are seen to be the same. The on-diagonal elements gradually fall off, while the off-diagonal elements increase. An interesting point is that the measured off-diagonal elements in some cases take on negative values, while the simulated elements, although following the same trend, follow a smoother trajectory and never go negative. Equation (29) illustrates that the $T_{21}$ and $T_{12}$ need not be positive definite when they are determined from multiple launches. However, apparently for the chosen values these elements are positive. This seems to indicate that the negatives of Fig. 2 are due to measurement noise and are not truly negative despite the multiple launch measurement technique. It is clear, however, that the matrix elements are much more noise resistant when determined from a transfer function than

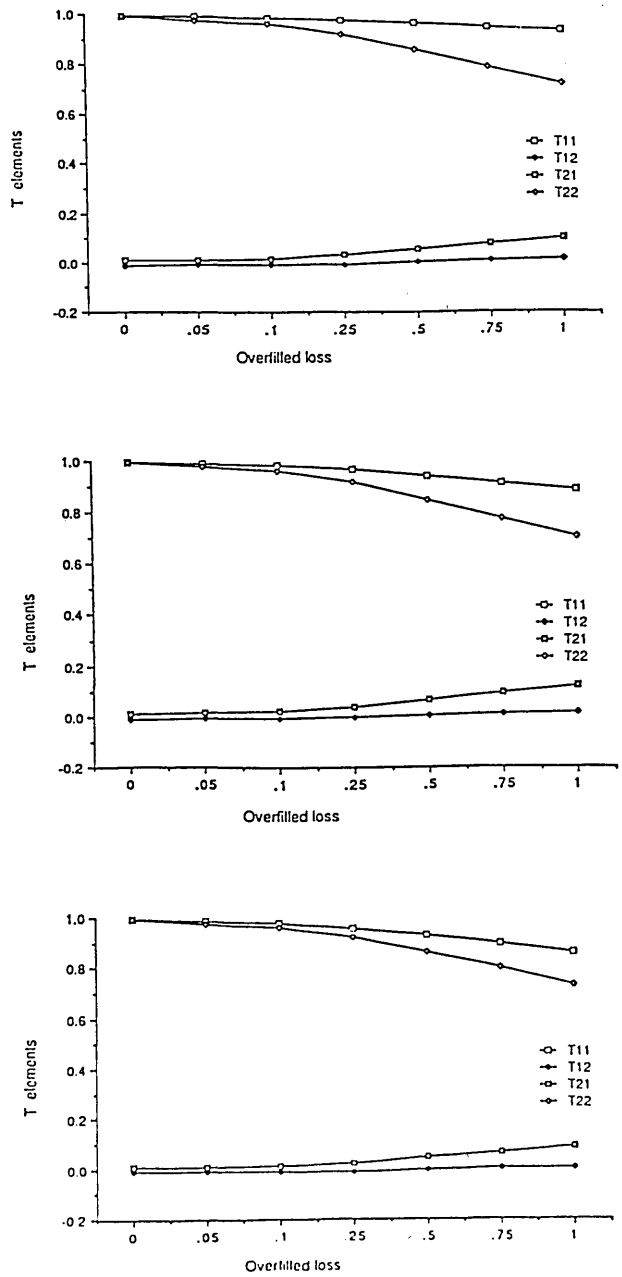


Fig. 4. Elements of transfer matrices predicted by Eq. (29) using the transfer function of Eq. (30) in Eq. (28), for the launch combination of $k_1 = 2.64$ and $k_2 = 2.88$, for seven different overfilled loss values with three different values of $\tau$ (0.05,0.1,0.2) for each loss where (a) corresponds to $\tau = 0.05$, (b) corresponds to $\tau = 0.1$, and (c) corresponds to $\tau = 0.2$.

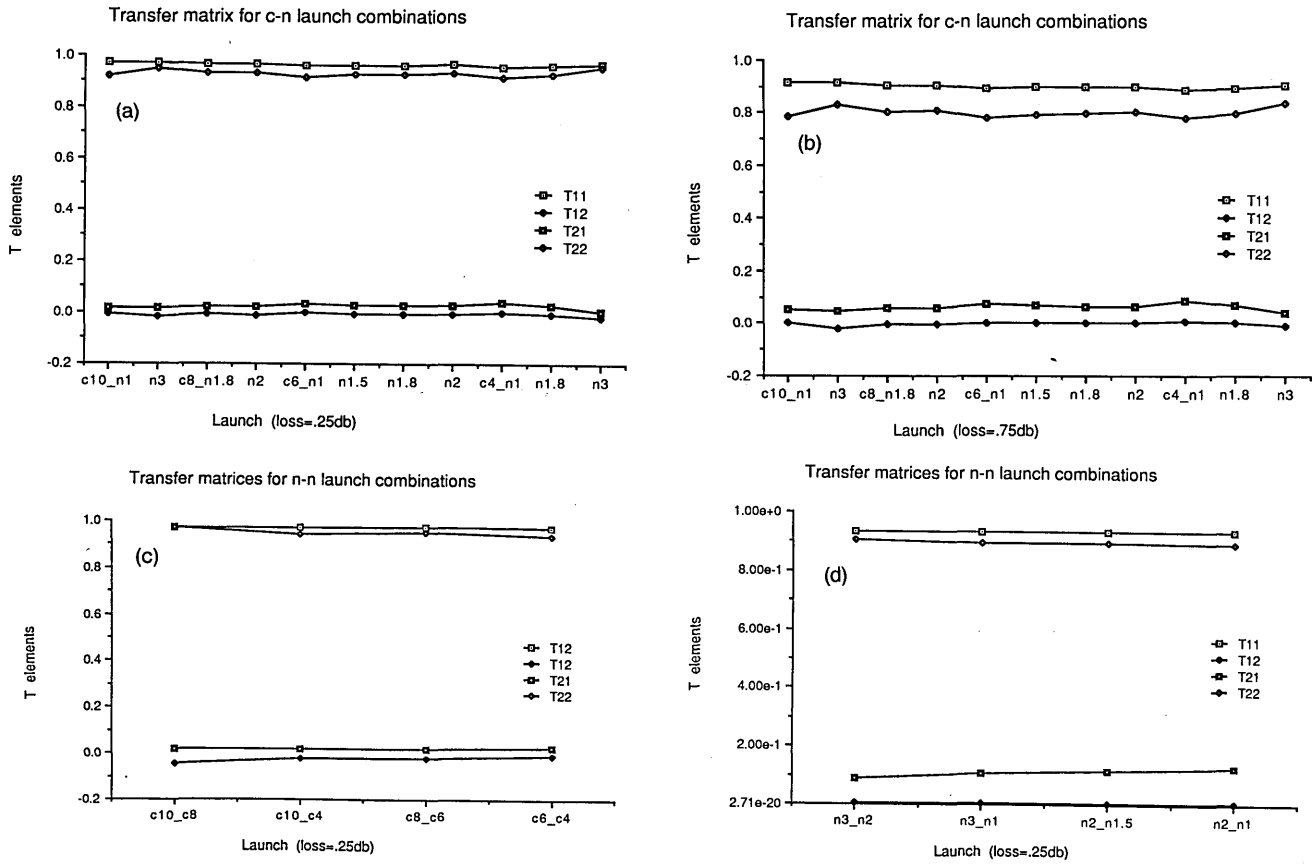


Fig. 5. Plots showing the dependence of matrix elements on launch conditions as predicted by Eq. (29) where abscissa shows the different combinations, with $c$ and $n$ denoting central and noncentral excitations, respectively, and the number after $c$ or $n$ isthe value of $k$ from Eq. (9), where (a) and (b) are for central, noncentral combinations and (c) and (d) are for central–central and noncentral–noncentral excitations, respectively.

when they are directly measured. Another point evident from comparison of Fig. 4 is that, although the matrix elements exhibit dependence on $\tau$, the dependence is not dramatic. That is to say, the matrix elements calculated from a transfer function are stable to bounded uncertainties in the determination of $\alpha_0$ and $\tau$.

Figures 5 illustrate the dependence of the transfer matrix elements derived from the transfer function on the different launches used to measure the transfer matrix as per Eq. (29). An interesting point noted from Figs. 5(a) and (b), with mixed central and noncentral launches, is that the jitter on each of the curves for the matrix elements is about the same regardless of the average value of the element. The fluctuations are therefore much more violent for the small $T_{12}$ and $T_{21}$ elements. Indeed, the jitter is sufficient to drive $T_{12}$ negative for various launch conditions. This is indeed the essence of the problem with the measured transfer matrices. Indeed, in Fig. 5(c), where different central excitations are used, $T_{12}$ can become considerably negative. In the case of Fig. 5(d), however, where only noncentral excitation is employed, all the elements seem more stable and $T_{12}$ remains essentially zero. This should not be taken as being indicative of all noncentral launch combinations, as no attempt was made in Figs. 5 to systematically trace out of the 2-D launch space.

Figures 6 illustrate the dependence of the measured matrix elements on variations in launch conditions. As it is a very tall task to refind a launch site with micron or submicron accuracy, it is well expected that reasonably large variation in the $k_1$ and $k_2$ values of Eq. (19) can occur. Therefore, the plots of Fig. 6 illustrate the variation of the matrix elements of Eq. (28) (matrix elements calculated form a single launch) with the input modal distribution, as can be characterized by $k_1$ and $k_2$. Although neither of the plots exhibit rapid fluctuations, both indicate explicitly that for certain input distributions, elements of the transfer matrix can be negative.

Figures 7 illustrate the more realistic case of two launch transfer matrix determinations. Here what is plotted are the elements of the transfer matrix, as predicted by Eq. (29), as a function of $k_1$ ($k_2$) for a fixed value of $k_2$ ($k_1$). Here, no negative values of transfer matrix elements are observed, unlike the cases depicted in Figs. 6. In the above examples, it has been assumed that the transfer function can somehow be determined.

Indeed, procedure for determining the $\alpha_0$ and $\tau$ of Eq. (31) from experiment can be carried out as follows.

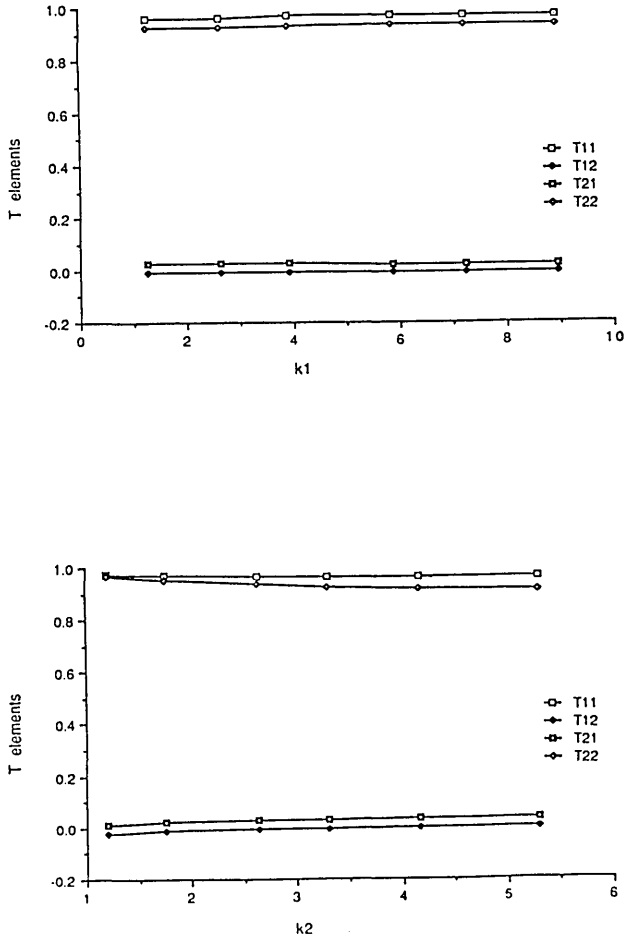


Fig. 6. Plots showing the variation of matrix elements derived from a transfer function with launch condition for (a) a transfer function found from a central excitation and (b) a transfer function found from a noncentral excitation.

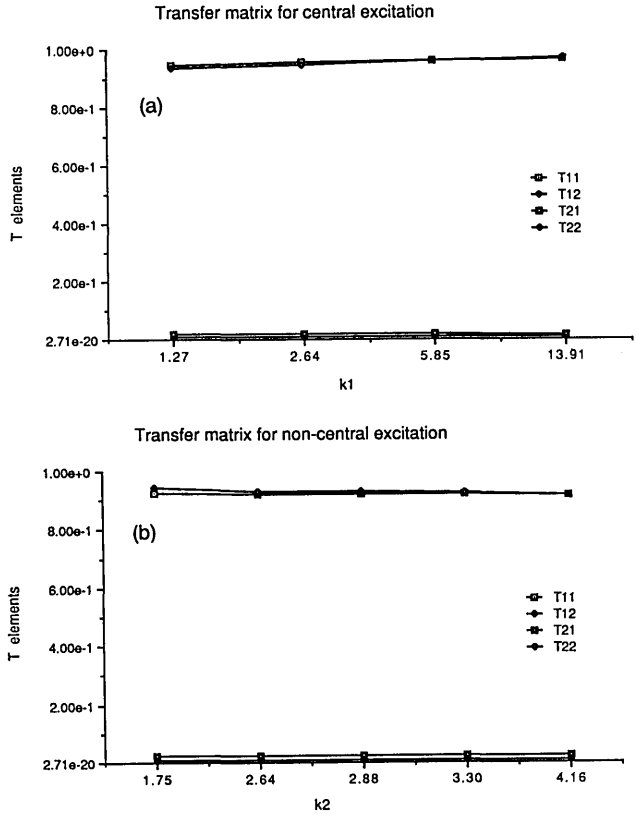


Fig. 7. Plots showing the dependence of the matrix elements for variations in launch conditions where in (a) $k_1 = 2.64$ is fixed and $k_2$ is the abscissa and in (b) $k_2 = 2.88$ is fixed and $k_1$ is allowed to vary.

First, one notes that the loss $L$ for overfilled excitation can be expressed as

$$L = 2\alpha_0 V^2 \tau^2 (1 + 2\tau)\left\{1 - 2\tau\left[1 - \exp\left(-\frac{1}{2\tau}\right)\right]\right\} \qquad (32)$$

where Eqs. (26) and (28) have been used to obtain Eq. (32). Equation (31) serves as the first of two equations needed to uniquely determine $\alpha_0$ and $\tau$. A second relation can be obtained by using Eq. (16) in Eq. (6) with the form adopted from Eqs. (30) and (31). What this gives is an expression for the near field intensity exiting a component, given a known input. As $\alpha_0$ and $\tau$ are characteristics of the component and not of the launch, it should not matter which launch is employed. Indeed, further discussion as well as experimental verification of this point are given in another work.[10] The point here is that, if a near field intensity distribution has been stored for any launch condition, Eq. (31) together with a fitting procedure may be used to determine $\alpha_0$ and $\tau$. A way to do this is to use Eq. (32) to eliminate $\alpha_0$ from Eq. (31) and then fit with $\tau$. Indeed, this has been done for the experimental cases of Fig. 2. The results are summarized in Table II. Here measured data are listed in the first row, matrices are predicted using the form of Eq. (29) in the second, and the matrices are predicted from Eq. (28) for the central $k$ in the third column and for the noncentral $k$ in the fourth column. The fit seems satisfactory and there does not seem to be any systematic skew in the predicted matrices with respect to the experimental data.

## VI. Conclusions

The launch dependence of the transfer matrix is a serious measurement problem. The results presented in this work show that the problem is a fundamental one. The use of a transfer function with experimentally determined parameters seems to be a preferable method of generating a meaningful characterization of a component. The transfer function technique, however, requires that a form for a coupling function be proposed and verified. Further discussion of the herein proposed couling function will be given elsewhere.[10]

## References

1. G. T. Holmes, "Estimation of Concatenated System Response Based on Measured Transfer Functions for Low and High Order Modes," in *Technical Digest Seventh European Conference on Optical Communication*, Copenhagen (1981), 3.4-1–3.4-4.
2. A. R. Mickelson, M. Eriksrud, S. Aamlid, and N. Ryen, "Role of the Fusion Splice in the Concatenation Problem," IEEE/OSA J. Lightwave Technol. **LT-2**, 126–138 (1984).

**Table II. Comparisons of Measured Matrices with those Predicted for Various Excitations**

| | $T_{11}$ | $T_{12}$ | $T_{21}$ | $T_{22}$ |
|---|---|---|---|---|
| $T_m$ | .9710 | .0020 | .0410 | .9270 |
| $T(m)$ | .9904 | -.0058 | .0154 | .9601 |
| $T(1)$ | .9870 | .0083 | .0063 | .9978 |
| $T(2)$ | .9451 | .0046 | .0163 | .9588 |

(a) $L = .067$ dB $\tau = .055$
$k_1 = 4.15$ $k_2 = 4.35$

| | $T_{11}$ | $T_{12}$ | $T_{21}$ | $T_{22}$ |
|---|---|---|---|---|
| $T_m$ | .9380 | -.0130 | .0870 | .9240 |
| $T(m)$ | .9769 | -.0012 | .0374 | .9218 |
| $T(1)$ | .9683 | .0170 | .0204 | .9580 |
| $T(2)$ | .9203 | .0108 | .0389 | .9215 |

(b) $L = .19$ dB $\tau = .07$
$k_1 = 2.13$ $k_2 = 4.72$

| | $T_{11}$ | $T_{12}$ | $T_{21}$ | $T_{22}$ |
|---|---|---|---|---|
| $T_m$ | .9730 | -.0380 | .0360 | .9500 |
| $T(m)$ | .9722 | .0004 | .0398 | .9011 |
| $T(1)$ | .9643 | .0243 | .0258 | .9437 |
| $T(2)$ | .9046 | .0150 | .0531 | .8982 |

(c) $L = .27$ dB $\tau = .075$
$k_1 = 3.04$ $k_2 = 4.63$


3. A. R. Mickelson, O. Klevhus, and M. Eriksrud, "Backscatter Readout from Serial Microbending Sensors," IEEE/OSA J. Lightwave Technol. **LT-2,** 700–709 (1984).
4. G. Evers, "Mode Transmission Matrices for Fibre-Optic Connectors," Electron Lett. **21,** 401–402 (1985).
5. G. Evers and U. Unrau, "Assessment of Modal Effects in Local Area Networks," Electron Lett. **22,** 859–861 (1986).
6. G. Evers, "Calculation and Measurement of Mode Transition Matrices for Differential Mode Attenuation and Differential Mode Delay Characterization of Optical Fibers," Opt. Eng. **27,** 179–186 (1988).
7. D. Marcuse, *The Theory of Dielectric Optical Waveguides* (Academic, New York, 1974).
8. See, for example, A. R. Mickelson and A. Weierholt, "Modal Noise Limited Signal to Noise Ratios in Multimode Optical Fibers," Appl. Opt. **22,** 3084–3089 (1983).
9. A. R. Mickelson and M. Eriksrud, "Mode-Continuum Approximation in Optical Fibers," Opt. Lett. **7,** 572–574 (1982).
10. S. Yang, D. R. Hjelme, I. P. Januar, I. P. Vayshenker, and A. R. Mickelson, "A Transfer Function Approach to Experimental Determination of Mode Transfer Matrices," submitted to Applied Optics.


●

NASA *continued from page 2978*

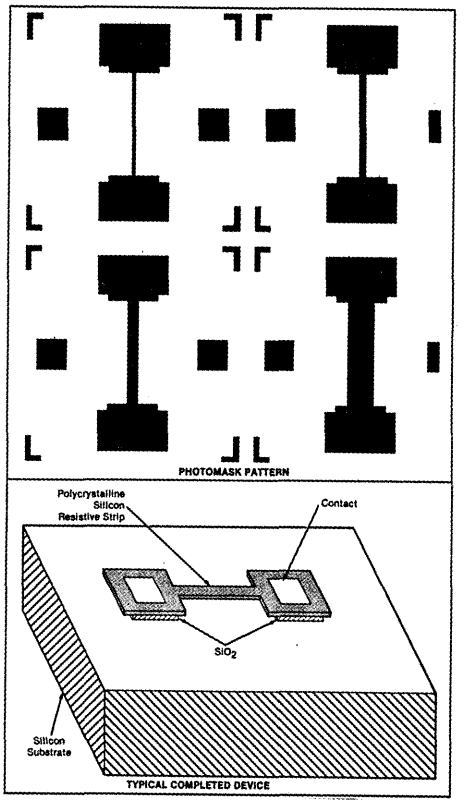


Fig. 3. Integrated circuit photomask pattern is used to make polycrystalline silicon strips of various widths and, therefore, of various electrical resistances and infrared characteristics. The strips are used as glow-bar resistors to calibrate infrared sensing instruments.

power dissipation. (Measurements have shown that the current vs voltage curve is fairly linear.)

A device can be made or used alone or as part of a flat panel or complicated multielement array of reference sources. A device or array is fabricated as follows:

1. A silicon substrate is oxidized to a depth of 10,000 Å.
2. A film of polycrystalline silicon 8000–10,000 Å thick is deposited on the oxide.
3. The polycrystalline silicon is doped with boron to obtain a resistance of 50–100 Ω/□.
4. The polycrystalline silicon is etched to form the pattern of resistor strips and contact areas (e.g., as shown in the upper part of Fig. 3).
5. The oxide is stripped from the exposed areas of the wafer and from under the beam(s), leaving only the oxide under the contact areas.
6. A thin film of aluminum is evaporated onto the entire water.
7. The pattern of contact pads is masked, and the aluminum is etched to leave only the portion in the contact areas.
8. The aluminum is alloyed to form the contacts.

A typical completed device is shown in the lower part of Fig. 3.

The self-passivating nature of the polycrystalline silicon adds to the reliability of the devices. The maximum operating temperature is over 1000 K, compared with the maximum of 600 K in prior devices. The power dissipation is only one-fourth that of the prior devices.

This work was done by G. Lamb, M. Jhabvala, and A. Burgess of Goddard Space Flight Center. Refer to GSC-13085.

*continued on page 3165*